Carbohydrate Polymers 97 (2013) 391–397

Contents lists available at SciVerse ScienceDirect

Carbohydrate Polymers

journal homepage: www.elsevier.com/locate/carbpol

Green synthesis of silver nanoparticles using 4-acetamido-TEMPO-oxidized curdlan

Jing-Kun Yan[a,b,*], Pan-Fu Cai[a], Xiao-Qiang Cao[a], Hai-Le Ma[a,b], Qi Zhang[a], Nan-Zi Hu[a], Yi-Zhang Zhao[a]

[a] School of Food & Biological Engineering, Jiangsu University, Zhenjiang 212013, Jiangsu, China
[b] Physical Processing of Agricultural Products Key Lab of Jiangsu Province, Zhenjiang 212013, Jiangsu, China

ARTICLE INFO

Article history:
Received 10 March 2013
Received in revised form 24 April 2013
Accepted 20 May 2013
Available online 27 May 2013

Keywords:
Curdlan
4-Acetamido-TEMPO
Green synthesis
Silver nanoparticles

ABSTRACT

A facile, simple, and eco-friendly method using 4-acetamido-2,2,6,6-tetramethypiperidine-1-oxyl radical-oxidized curdlan (Oc) as both reducing and stabilizing agents was developed for the fabrication of silver nanoparticles (AgNPs) from silver nitrate ($AgNO_3$). The structure, morphology, and particle size of the as-prepared AgNPs were investigated by ultraviolet-visible spectroscopy, transmission electron microscopy, energy dispersive X-ray spectrometry, X-ray diffraction, and dynamic laser light scattering. The well-dispersed AgNPs were sphere like with a mean diameter of 15 nm. Their formation was dependent on reaction duration, reaction temperature, Oc concentration, and $AgNO_3$ concentration. Fourier transform-infrared and Raman spectra demonstrated that the as-prepared AgNPs can readily bind covalently with the carboxylate groups of Oc through the strong monodentate interaction in the reaction medium.

1. Introduction

Nanotechnology is considered as the most advanced technology in the 21st century. It is closely related to physics, chemistry, biology, material science, and medicine. It has been widely used in biomedicine for the development of nanoparticle (NP)-based drug delivery systems, rapid pathogen detection, biomolecular sensing, and NP-based cancer diagnosis and therapy (Daaboul et al., 2010; Hallaj-Nezhadi, Lotfipour, & Dass, 2010; Miranda, Creran, & Rotello, 2010; Portney & Ozkan, 2006). In particular, silver (Ag) NPs are preferred over bulk metals because of their distinctive electrical, electronic, thermal, optical, magnetic, catalytic, sensing, and antimicrobial functionalities (Lara, Garza-Treviño, Ixtepan-Turrent, & Singh, 2011; Ravindran, Chandran, & Khan, 2012). Numerous methods, including chemical reduction (Lee & Meisel, 1982), thermal decomposition (Yang, Matsubara, & Xiong, 2007), laser ablation (Simakin, Voronov, Kirichenko, & Shafeev, 2004), and sonochemical synthesis (Salkar, Jeevanandam, Aruna, Koltypin, & Gedanken, 1999), have been utilized for the synthesis of AgNPs. Among these methods, chemical reduction using sodium borohydride and citrate as reducing and protecting agents, respectively, is the most common approach to prepare AgNPs (Evanoff & Chumanov, 2005).

The preparation of AgNPs using biopolymers has drawn considerable attention (Eby, Schaeublin, Farrington, Hussain, & Johnson, 2009; Matthew, Dickerson, Sandhage, & Naik, 2008; Xia, Monterio-Riviere, & Riviere, 2010). Under relatively mild conditions, biomacromolecules can be used as both reducing and stabilizing agents to synthesize high-yield and environment-friendly AgNPs in aqueous solution. As the most abundant polymers in the biosphere, natural polysaccharides are potential candidates for the preparation of AgNPs. Raveendran, Fu, and Wallen (2003) was the first to report the complete green synthesis of AgNPs using β-D-glucose and starch as reducing and stabilizing agents, respectively (Raveendran et al., 2003). Several polysaccharides, such as starch, cellulose, chitosan, dextran, heparin, and hyaluronan fibers, have been widely used as both reducing and stabilizing agents to fabricate AgNPs (Abdel-Mohsen et al., 2012; Bankura et al., 2012; Chen, Wang, Zhang, & Jin, 2008; Kemp & Linhardt, 2010; Raveendran et al., 2003; Wei & Qian, 2008).

Curdlan is a neutral bacterial exopolysaccharide composed primarily of linear β-(1,3)-glycosidic linkages. It has been widely applied in the food and pharmaceutical industries because of its unique gelling properties and important bioactivities. However, the water-insolubility of curdlan limits its practical applications. Carboxymethylation has become one of the most important and effective methods used to improve the functional properties of curdlan (Jin, Zhang, Yin, & Nishinari, 2006). Carboxymethyl curdlan (CMc) can act as both reducing and stabilizing agents for the synthesis of AgNPs because of its hydroxyl and carboxylic groups

* Corresponding author at: School of Food & Biological Engineering, Jiangsu University, Zhenjiang 212013, Jiangsu, China. Tel.: +86 15952819661.
E-mail address: jkyan_27@163.com (J.-K. Yan).

0144-8617/$ – see front matter © 2013 Elsevier Ltd. All rights reserved.
http://dx.doi.org/10.1016/j.carbpol.2013.05.049

(Leung, Wong, & Xie, 2010; Wu, Zhang, & Zhang, 2012). However, the preparation of CMc usually depends on the use of the esterification reagent chloroacetic acid, which is potentially toxic to the environment. Recent studies have reported the regioselective oxidation of the C6 primary hydroxyl groups of curdlan using 2,2,6,6-tetramethypiperidine-1-oxyl radical (TEMPO) or its analog as a catalyst under mild conditions (Tamura, Wada, & Isogai, 2009; Tamura, Hitora, Saito, & Isogai, 2010; Watanabe, Tamura, Saito, Habu, & Isogai, 2012). TEMPO- or 4-acetamido-TEMPO-oxidized curdlan (Oc) contains numerous hydroxyl and carboxylic groups. Thus, similar to CMc, Oc can also be used as both reducing and stabilizing agents for the green synthesis of AgNPs.

This study aims to develop a novel approach for the green synthesis of AgNPs using 4-acetamido-TEMPO-Oc as both reducing and stabilizing agents under various reaction conditions. The structure, particle size, and morphology of the as-prepared AgNPs were investigated by ultraviolet-visible (UV-vis) spectroscopy, transmission electron microscopy (TEM), energy dispersive X-ray spectrometry (EDX), X-ray diffraction (XRD), dynamic light scattering (DLS), Fourier transform-infrared spectroscopy (FT-IR), and Raman spectroscopy. The formation mechanism of the AgNPs was also discussed in this study.

2. Materials and methods

2.1. Materials

Commercial curdlan (DP_w 6790) was obtained from Wako Pure Chemical Corporation (Osaka, Japan). 4-Acetamido-TEMPO-Oc was synthesized following the method described by Tamura et al. (Tamura et al., 2010). The carboxylate (COO^-) content of Oc was determined to be 4.87 mmol/g using electric conductimetry titration (Saito, & Isogai, 2004). 4-Acetamido-TEMPO and silver nitrate ($AgNO_3$) were purchased from Sigma–Aldrich Chemical Corporation (St. Louis, MO, USA). All other chemicals and solvents were of laboratory grade and used without further purification.

2.2. In situ synthesis of AgNPs

AgNPs were synthesized by direct mixture of $AgNO_3$ and 4-acetamido-TEMPO-Oc in aqueous solution. Briefly, 1.0 mL each of different concentrations of $AgNO_3$ solution (1.0–100 mM) and Oc (0.1–2.0 mg/mL) were mixed under continuous stirring at different temperatures (70–100 °C) and durations (30–120 min) in the dark. The progression of the reaction was monitored by UV-vis absorption.

2.3. Size-exclusion chromatography with multi-angle laser-light scattering (SEC-MALLS) analysis

The weight-average molecular weight (M_w) and radius of gyration ($\langle S^2 \rangle z^{1/2}$) of the Oc in 0.1 M NaCl were determined by SEC-MALLS (DAWN HELEOS II, λ = 658 nm: Wyatt Technologies Corporation, USA). A differential refractive index detector (RI, 2414, Waters Corporation, USA) and a 515 pump (Waters Corporation, USA) with a SEC column (OHpak SB-806 M HQ, 8 mm $\Phi \times$ 30 cm, Shodex, Japan) in 0.1 M NaCl at 25 °C were used. The eluent was 0.1 M aqueous NaCl at a flow rate of 0.5 mL/min. The polysaccharide solution and solvent were purified by a 0.45 μm filter and then degassed before use. The injection volume was 100 μL with a concentration of 1.0 mg/mL for the sample. The specific RI increment (dn/dc) of Oc in 0.1 M NaCl was 0.125 mL/g (Shibata, Yanagisawa, Saito, & Isogai, 2006). The Astra software was utilized for data acquisition and analysis.

2.4. Characterization

The UV-vis spectra of the as-prepared AgNPs using Oc were recorded in a Varian cary 100 spectrophotometer (Varian Co., USA) from 300 nm to 600 nm. FT-IR spectra were recorded from 500 cm^{-1} to 4000 cm^{-1} using a Nexus 670 FT-IR instrument (Thermo Nicolet Co., USA). Raman spectra were recorded from 500 cm^{-1} to 3500 cm^{-1} using a DXR Raman microscope (Thermoelectron Co., USA) equipped with He–Ne laser (532 nm, 10 mW). The as-prepared AgNPs were observed using a Malvern Zetasizer Nano (3000 SHA Malvern Instruments Ltd., UK) at 632.8 nm and 90° scatterring angle. The average particle size was measured based on the DLS analysis. TEM (JEM-2100, JEOL Ltd., Japan, 200 kV) was used to characterize the size and morphology of the as-prepared AgNPs. For the preparation of test samples, a drop of the sample solution was placed on 300 mesh carbon-coated copper grids and then dried at room temperature for 30 min. An EDX spectroscope (Inca Energy-350, Oxford Co., UK) attached to an SEM (JSM-7100F, JEOL Ltd., Japan) was used to determine the elemental composition of the AgNPs. A wide-angle XRD instrument (D8-Advance, Bruker Co., Germany) was used to characterize the critical structure of the AgNPs. XRD patterns with Cu K_α radiation (λ = 0.15406 nm) at 40 kV and 40 mA were recorded in the region of 2θ from 30° to 80° with a step speed of 4 °/min.

3. Results and discussion

3.1. Chain conformation of Oc

SEC combined with MALLS is a convenient approach for the determination of M_w, $\langle S^2 \rangle z^{1/2}$, and the polydispersity (M_w/M_n) of polymers in solution. Fig. 1a shows the SEC chromatogram of Oc in 0.1 M aqueous NaCl at 25 °C. Based on the results of SEC-MALLS, the values of M_w, $\langle S^2 \rangle z^{1/2}$, and M_w/M_n for Oc were calculated to be 1.2×10^5 g/mol, 59.8 nm, and 1.38, respectively. The single peak suggested the absence of aggregation or polysaccharide of different structures in the aqueous solution. The SEC-MALLS chromatogram can produce the function of $\langle S^2 \rangle z^{1/2} = f \cdot M_w^{\alpha}$. The power law of the former can be estimated from many experimental points in the SEC chromatogram (Mendichi, Giammonab, Cavallarob, & Giacometti Schieronia, 2000). The exponent may provide additional insights into the conformation of the polymer solution. The exponents of 0.33, 0.50 to 0.60, and 1.0 often reflect the chain shape for the adaptation of sphere, random coil, and rigid rod, respectively (Kato, Okamoto, Tokuya, & Takahashi, 1982; Picton, Bataille, & Muller, 2000). Fig. 1b shows the log-log plot of $\langle S^2 \rangle z^{1/2}$ against M_w for the Oc in 0.1 M aqueous NaCl at 25 °C. The obtained α value of 0.71 suggested that the Oc in 0.1 M NaCl aqueous solution was in the state between random coil and rigid rod, which was exhibited as a semi-flexible chain conformation. The conversion of C6-CH_2OH groups to C6-COO^- groups significantly destroyed the intra- and inter-molecular hydrogen bonds and reduced the main-chain hydrophobicity that was indispensable to stabilize the triple strand of curdlan. Furthermore, the introduction of C6-COO^- groups enhanced the steric hindrance between the polymer chains, leading to the relatively expanded random coil conformation of Oc.

3.2. Preparation of AgNPs

AgNPs were prepared using Oc as both reducing and stabilizing agents. The abundance of COO^- groups in Oc enriched the Ag^+ ions in solution, thus facilitating the formation of AgNPs. The preparation of Oc-stabilized AgNPs is almost similar to that of AgNPs using CMc (Leung et al., 2010). The different factors affecting the

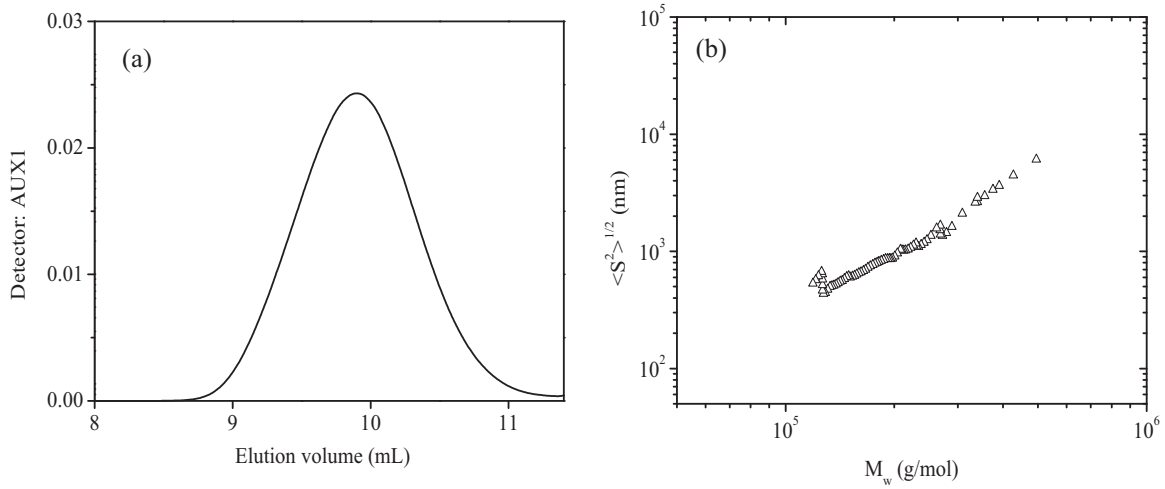

Fig. 1. (a) SEC chromatogram of the Oc in 0.1 M NaCl aqueous solution at 25 °C by SEC-MALLS. "Detector: AUX1" represents a relative concentration; (b) plot of $\langle S^2 \rangle z^{1/2}$ vs. M_w in double logarithmic coordinate for the Oc in 0.1 M NaCl aqueous solution at 25 °C by SEC-MALLS.

reduction efficiency and stability as well as the shape and size of the formed AgNPs are given below.

3.2.1. *Effect of reaction duration*

Fig. 2a shows the UV-vis absorption spectra of AgNP colloidal solutions prepared from 1 mL of Oc (1 mg/mL) with 1 mL of $AgNO_3$ solution (10 mM) at 100 °C for different durations. A slight absorption band at approximately 410 nm appeared after 30 min of reaction. This band became significantly visible after 45 min of reaction, suggesting the presence of spherical AgNPs in the system (Jradi et al., 2010). The peak was symmetrical and showed no obvious absorption from 450 nm to 600 nm, indicating that

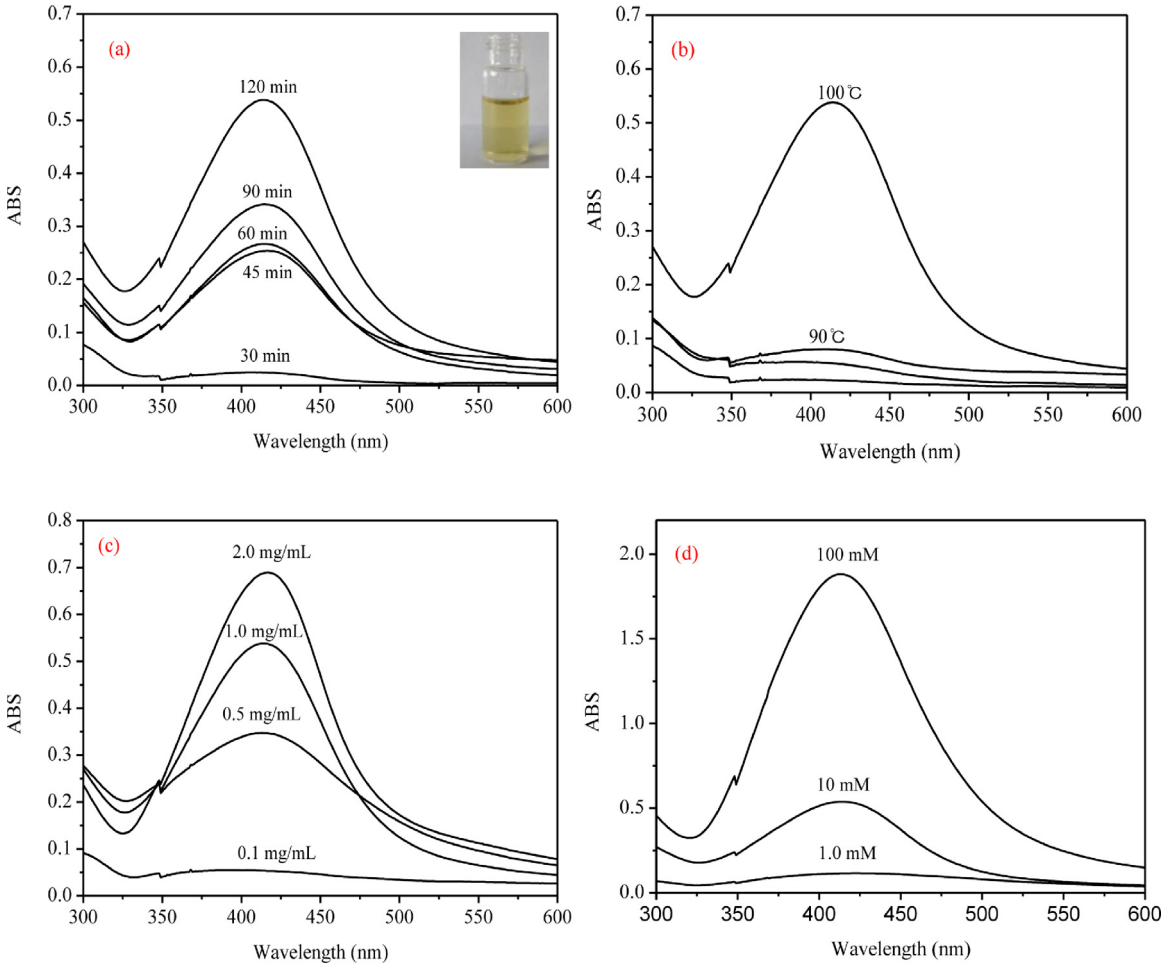

Fig. 2. UV-vis absorption spectra for the AgNPs prepared on different (a) durations, (b) temperature, (c) concentrations of $AgNO_3$, and (d) concentrations of Oc. The inset in *A* is the photo of the Oc-Ag nanoparticles.

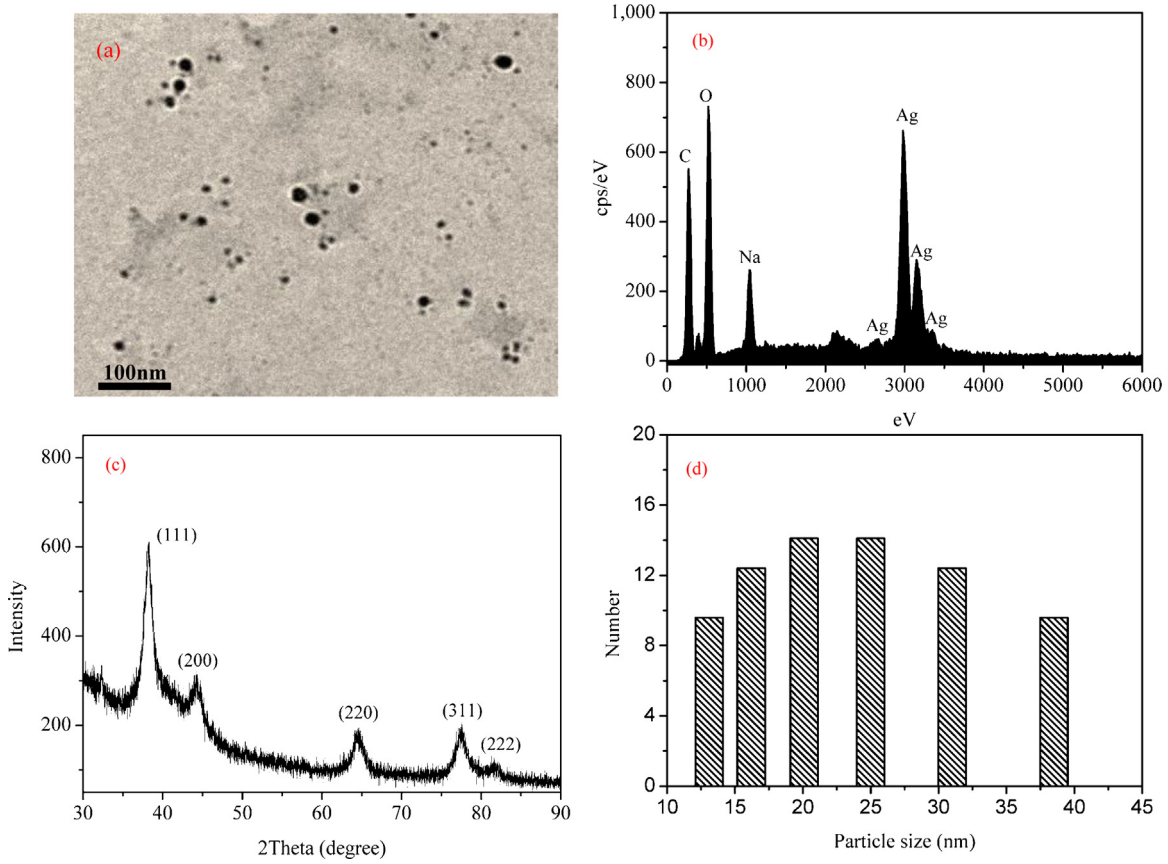

Fig. 3. (a) Typical TEM image, (b) EDX spectrum from SEM, (c) XRD pattern, and (d) particle size distribution from DLS analysis of AgNPs prepared by 1.0 mg/mL Oc and 10 mM $AgNO_3$.

negligible aggregation occurred in this reactive system (Chen et al., 2008). Meanwhile, the color of the Oc-$AgNO_3$ solution changed from colorless to golden yellow, further indicating the formation of AgNPs. The UV-vis spectra of Oc showed that the absorbance at 410 nm became stronger with prolonged heat treatment, indicating that several Ag ions were reduced and used for cluster formation. However, the reaction duration for AgNP formation using Oc was longer than that using CMc. This difference may be attributed to the different structures and chain conformations of Oc and CMc.

3.2.2. *Effect of reaction temperature*

Fig. 2b shows the UV-vis spectra of the AgNPs prepared at different temperatures under the following reaction conditions: Oc and $AgNO_3$ concentrations of 1 mg/mL and 10 mM, respectively, and reaction duration of 120 min. The results indicated that the reduction efficiency below 90 °C was not enough for the complete transformation of Ag^+ into AgNPs. The absorption band at ~410 nm was clearly observed when the reaction temperature was increased to 100 °C, which corresponded to the surface plasmon response (SPR) (Huang & Xu, 2010). This result indicated that Ag^+ was transformed into Ag^0. Thus, the preparation of AgNPs from Oc should be controlled at 100 °C or above.

3.2.3. *Effect of Oc concentration*

Fig. 2c shows the UV-vis spectra of the AgNPs prepared with different concentrations of Oc (0.1 mg/mL to 2.0 mg/mL) and 10 mM of $AgNO_3$ at 100 °C for 120 min. At a low Oc concentration of 0.1 mg/mL, Ag^+ was not sufficiently reduced and stabilized for the preparation of AgNPs. When the concentration of Oc increased from 0.1 mg/mL to 0.5 mg/mL, the absorption band appeared at ~410 nm, indicating the formation of AgNPs. When the concentration of Oc increased up to 2.0 mg/mL, the absorption intensity gradually increased and the shape of the absorption band became much narrower. These results revealed that the prepared AgNPs from Oc were spherical and monodisperse with decreased size (Hutter & Fendler, 2004). In the present study, 1.0 mg/mL of Oc in the reaction medium was enough for the preparation of AgNPs. Neither AgNP aggregation nor polymer phase separation was observed under this condition.

3.2.4. *Effect of $AgNO_3$ concentration*

Fig. 2d shows the UV-vis spectra of the AgNPs prepared using different concentrations of $AgNO_3$ (1–100 mM) and 1.0 mg/mL of Oc at 100 °C for 120 min. The intensity of the absorbance band at ~410 nm enhanced with increasing $AgNO_3$ concentration. This result indicated that the content of AgNPs in the reaction medium increased with increasing $AgNO_3$ concentration. In addition, the maximum plasmon absorption band at ~410 nm did not red shift. This result indicated that the size of the AgNPs remained unchanged with increasing $AgNO_3$ concentration because of the presence of Oc macromolecules. The concentration of $AgNO_3$ suitable for the preparation of AgNPs was found to be 10 mM. At this concentration, the aggregation of AgNPs was prevented. In addition, high Ag concentrations favored the thermal process, which led to less selectivity for the transformation of isotropic Ag seeds into anisotropic triangular prisms (Xue, Meĭtraux, Millstone, & Mirkin, 2008).

3.3. *Characterization of AgNPs*

Fig. 3a shows the typical TEM image of the AgNPs (Oc-AgNPs) synthesized with 1.0 mg/mL Oc and 10 mM $AgNO_3$ at 100 °C for 120 min. As shown in the figure, most of the particles were isotropic

and reasonably monodisperse. Almost all of the nanoparticles were well separated with no signs of agglomeration. The average particle size obtained from the TEM micrograph was approximately 15 nm. The size-dependent SPR and the yellow color of the as-prepared AgNPs indicated that a mean size of ~15 nm was reliable (Huang and Xu, 2010). The TEM result was in good agreement with the SPR result for the nanoparticle size. Previous studies indicated that the particle size of Oc-AgNPs synthesized by Oc is almost similar to those synthesized by lentinan (12 nm) (Li, Zhang, Xu, & Zhang, 2011), dextran (5–10 nm) (Bankura et al., 2012), and marine polysaccharide (13 nm) (Venkatpurwar, & Pokharkar, 2011), but less than those prepared by CMc (40 nm) (Leung et al., 2010). The shape remained sphere like in the present study and in previous studies.

Fig. 3b shows the EDX analysis of the Oc-AgNPs. The EDX spectrum showed a strong and typical optical absorption peak at approximately 3000 eV, which was attributed to the SPR of the metallic Ag nanocrystals (Magudapatty, Gangopaghyayrans, Panigrahi, Nair, & Dhara, 2001). This result indicated that AgNPs were formed in the reaction medium. In addition, the presence of Ag, C, and O elements also indicated that the nanocomposite consisted of Oc and AgNPs.

XRD analysis was performed to determine and confirm the crystalline nature of AgNPs. Fig. 3c shows the XRD spectrum of the Oc-AgNPs. The peaks at approximately 38.3°, 44.4°, 65.0°, 77.8° and 82.1° were attributed to the (1 1 1), (2 0 0), (2 2 0), (3 1 1) and (2 2 2) planes of the cubic structure of Ag (He, Yao, Xie, Gao, & Pang, 2001). No peaks related to other crystalline phases were found. Among them, the diffraction peak at 38° was the only highly intense peak. Moreover, the ratio between the (2 2 0) and (1 1 1) peaks was much lower than the standard value (0.1 versus 0.4). These results further demonstrated that the preferred orientation for the calcined AgNPs was assigned to the (1 1 1) lattice plane.

Fig. 3d shows a histogram of the particle size distribution by DLS, with a mean particle diameter of 27 nm. The diameter appeared a little difference from the result determined by TEM measurement. This was mainly due to the process involved in the preparation of samples. In the case of the TEM method, a TEM image depicts the size at the dried state of the sample, whereas DLS method involves the measurement of size in the hydrated state. In other words, the size determined by TEM is an actual diameter (dry state) of the nanoparticles, whereas the size measured by the laser light scattering method is a hydrodynamic diameter (hydrated state), and therefore the nanoparticles will have a larger hydrodynamic volume due to solvent effect in the hydrated state (Gao et al., 2008). Thus, the size of Oc-AgNPs measured by DLS method was larger than the size observed by TEM method.

3.4. Formation mechanism of AgNPs

Solutions of polymers, such as linear and dendritic polymers, polyhydroxylated macromolecules, and polysaccharides, can be used for the green synthesis of nanoparticles. In particular, modified polysaccharides have been widely applied as both reducing and stabilizing agents for the green synthesis of AgNPs.

The C6-Oc prepared using 4-acetamido-TEMPO could act as a template for the complexation of Ag ions because of its numerous hydroxyl and carboxylic groups. Fig. 4 depicts a schematic of the green synthesis of AgNPs by Oc. Curdlan was first oxidized by 4-acetamido-TEMPO to prepare water-soluble derivatives containing reducing and carboxyl groups. The triple helical chain of curdlan was converted to a semi-flexible chain. The negatively charged solubilized Oc facilitated the attraction of Ag^+ ions to the polymeric chains by electrostatic attractive forces. Some Ag^+ ions were reduced by the available reducing groups of Oc. The produced Ag^0 atoms acted as nucleation centers and further catalyzed the

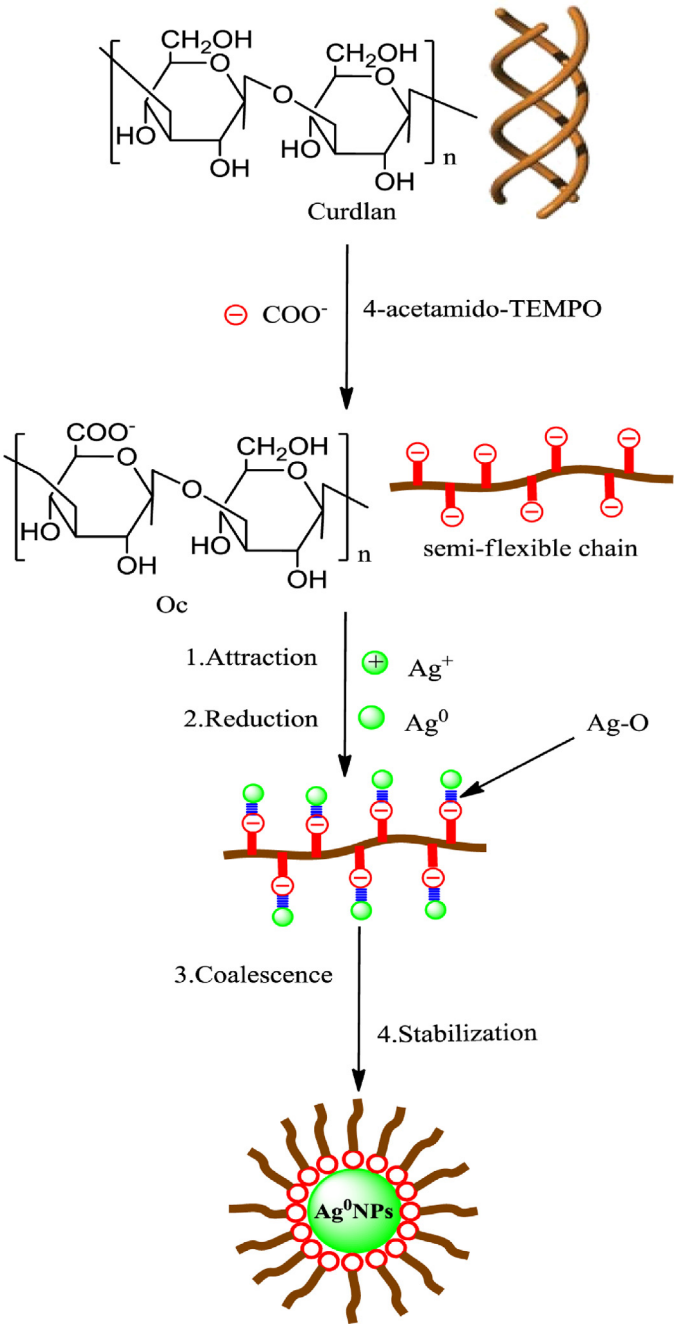

Fig. 4. Schematic outline of the green synthesis of AgNPs by using Oc. (For interpretation of the references to color in figure legend, the reader is referred to the web version of the article.)

reduction of the remaining Ag^+ ions to Ag^0. Subsequently, Ag clusters were formed by the coalescence of Ag^0 atoms. The surface Ag^+ ions were again reduced, during which aggregation did not cease until high values of nuclearity were attained, which resulted in larger particles. The process was stabilized by the interaction with the polymer, thereby preventing further coalescence (Goia, 2004).

The FT-IR and FT Raman spectra of AgNPs were recorded to determine the interaction between AgNPs and Oc molecules. Fig. 5a shows the FT-IR spectra of the Oc and Oc-AgNPs. The Oc spectrum showed that the absorption bands at 1620 and 1420 cm^{-1} were attributed to the asymmetrical and symmetrical COO^- stretching vibrations, respectively (Donati et al., 2009). The Oc-AgNP spectrum showed that a new absorption band at approximately 1384 cm^{-1},

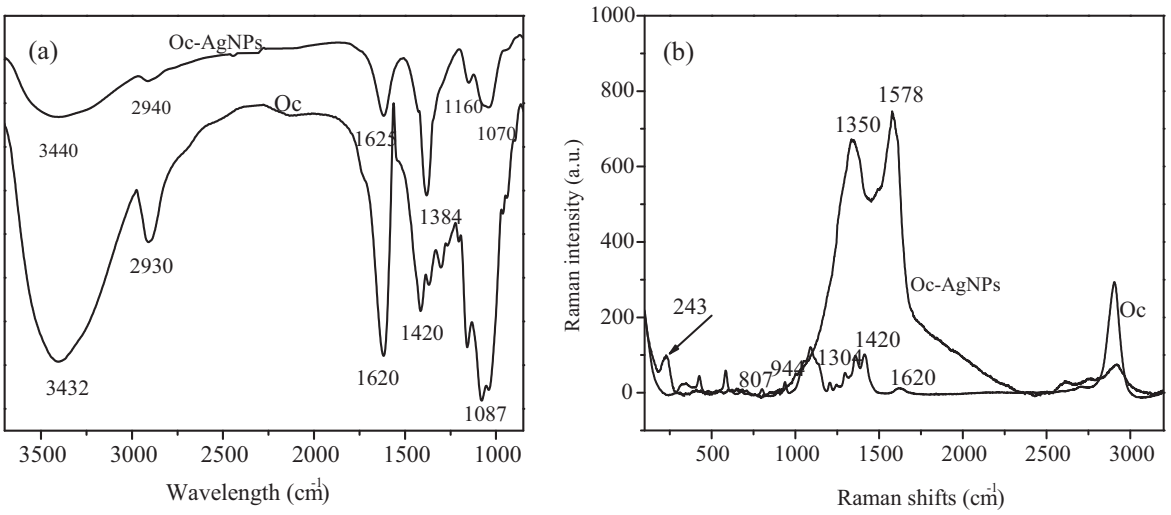

Fig. 5. (a) FT-IR and (b) FT Raman spectra of Oc power and Oc-stabilized AgNPs.

which was considered to be characteristic of carboxylic groups adsorbed on Ag, corresponded to the symmetric stretching mode of COO^- groups. In addition, the slight red shift from 1620 cm^{-1} to 1625 cm^{-1} was attributed to the asymmetrical COO^- stretching vibration, proving the interaction between the Oc molecules and AgNPs. The modes of monodentate, chelating bidentate, bidentate bridging, and ionic interaction are often used to evaluate the type of interaction between COO^- groups and metal nanoparticles by calculating the wave number difference (Δ) between the asymmetrical and symmetrical COO^- stretching vibrations. The Δ ranges of <110, 140–190, and 200–320 cm^{-1} often reflect that the interaction type is chelating bidentate, bidentate bridging, and monodentate, respectively (Liu, He, Durham, Zhao, & Roberts, 2008). The Δ value was calculated to be 241 cm^{-1} (1625–1384 cm^{-1}), indicating that the type of interaction between the COO^- groups and AgNPs was monodentate. This result is similar to those of previous studies (Wu et al., 2012).

Fig. 5b illustrates the FT Raman spectra of Oc and Oc-AgNPs. The absorption band at approximately 243 cm^{-1} in the Oc-AgNP spectrum was attributed to the Ag-O stretching vibration (Biswas, Kappor, Mahal, & Mukherjee, 2007). This result further suggested that the interaction between Ag and the COO^- groups of Oc molecules was linked by a chemical bond. In addition, the strong and sharp peaks at 1350 and 1578 cm^{-1} suggested the direct binding of the COO^- group with the Ag surface (Biswas et al., 2007). The FT-IR and FT Raman spectra indicated that the COO^- groups of Oc molecules covalently and directly interacted with AgNPs by monodentate interaction in aqueous solution.

4. Conclusions

C6-Oc, exhibited as a semi-flexible chain in aqueous solution, was utilized as both reducing and stabilizing agents for the green synthesis of AgNPs. The formation of AgNPs was affected by reaction duration, reaction temperature, Oc concentration, and $AgNO_3$ concentration. It was monitored via color and UV-vis analyses. The results confirmed that well-dispersed AgNPs were prepared by hybridization of 1.0 mg/mL Oc and 10 mM $AgNO_3$ at 100 °C for 120 min. The particle size and morphology of the AgNPs were determined by TEM, EDX, XRD, and DLS analyses. The as-prepared AgNPs were spherical and monodispersed with a mean particle size of approximately 15 nm. The abundance of hydroxyl and COO^- groups facilitated the complexation of Ag ions. The FT-IR and FT Raman spectra indicated that the interaction between the COO^- groups of Oc molecules and AgNPs was monodentate. Oc-capped AgNPs can be explored as a novel fluorescent sensing platform for nucleic acid detection. The results of the present study provide important insights into the interaction of bovine serum albumin. Further investigations are currently underway.

Acknowledgements

This work was supported financially by the Priority Academic Program Development (PAPD) of Jiangsu Higher Education Institutions, the China's Postdoctoral Science Fund Projects (2013M531292), School Foundation Financing Project of Jiangsu University (105DG129), the Open Foundation of Jiangsu Province Key Laboratory of Physical Processing on Agricultural Products (JAPP2010-7), Jiangsu university undergraduate innovation project (2012097) and Jiangsu university students' scientific research project (11A343).

References

Abdel-Mohsen, A. M., Hrdina, R., Burgert, L., Krylová, G., Abdel-Rahman, R. M., Krejčová, A., et al. (2012). Green synthesis of hyaluronan fibers with silver nanoparticles. *Carbohydrate Polymers*, *89*, 411–422.

Bankura, K. P., Maity, D., Mollick, M. M. R., Mondal, D., Bhowmick, B., Bain, M. K., et al. (2012). Synthesis, characterization and antimicrobial activity of dextran stabilized silver nanoparticles in aqueous medium. *Carbohydrate Polymers*, *89*, 1159–1165.

Biswas, N., Kappor, S., Mahal, H. S., & Mukherjee, T. (2007). Adsorption of CGA on colloidal silver nanoparticles: DFT and SERS study. *Chemical Physics Letters*, *444*, 338–345.

Chen, J., Wang, J., Zhang, X., & Jin, Y. (2008). Microwave-assisted green synthesis of silver nanoparticles by carboxymethyl cellulose sodium and silver nitrate. *Materials Chemistry and Physics*, *108*, 421–424.

Daaboul, G. G., Yurt, A., Zhang, X., Hwang, G. M., Goldberg, B. B., & Ünlü, M. S. (2010). High-throughput detection and sizing of individual low-index nanoparticles and viruses for pathogen identification. *Nano Letters*, *10*, 4727–4731.

Donati, I., Travan, A., Pelillo, C., Scarpa, T., Coslovi, A., Bonifacio, A., et al. (2009). Polyol synthesis of silver nanoparticles: Mechanism of reduction by alditol bearing polysaccharides. *Biomacromolecules*, *10*(2), 210–213.

Eby, D., Schaeublin, N., Farrington, K., Hussain, S., & Johnson, G. (2009). Lysozyme catalyzes the formation of antimicrobial silver nanoparticles. *ACS Nano*, *3*, 984–994.

Evanoff, D. D., & Chumanov, G. (2005). Synthesis and optical properties of silver nanoparticles and arrays. *ChemPhysChem*, *6*, 1221–1231.

Gao, F. P., Zhang, H. Z., Liu, L. R., Wang, Y. S., Jiang, Q., Yang, X. D., et al. (2008). Preparation and physicochemical characteristics of self-assembled nanoparticles of deoxycholic acid modified-carboxymethyl curdlan conjugates. *Carbohydrate Polymers*, *71*, 606–613.

Goia, D. V. (2004). Preparation and formation mechanisms of uniform metallic particles in homogeneous solutions. *Journal of Material Chemistry*, *14*, 451–458.

Hallaj-Nezhadi, S., Lotfipour, F., & Dass, C. R. (2010). Delivery of nanoparticulate drug delivery systems via the intravenous route for cancer gene therapy. *Pharmazie*, *65*, 855–859.

He, S., Yao, J., Xie, S., Gao, H., & Pang, S. (2001). Superlattices of silver nanoparticles passivated by mercaptan. *Journal of Physics D: Applied Physics*, *34*, 3425–3429.
Huang, T., & Xu, X. (2010). Synthesis and characterization of tunable rainbow colored colloidal silver nanoparticles using single-nanoparticle plasmonic microscopy and spectroscopy. *Journal of Materials Chemistry*, *20*, 9867–9876.
Hutter, E., & Fendler, J. H. (2004). Exploitation of localized surface plasmon response. *Advanced Materials*, *16*, 1685–1706.
Jin, Y., Zhang, H., Yin, M., & Nishinari, K. (2006). Comparison of curdlan and its carboxymethlated derivative by means of rheology, DSC, and AFM. *Carbohydrate Research*, *341*, 90–99.
Jradi, S., Balan, L., Zeng, X. H., Plain, J., Lougnot, D. J., & Royer, P. (2010). Spatially controlled synthesis of silver nanoparticles and nanowires by photosensitized reduction. *Nanotechnology*, *21*, 95605–95612.
Kato, T., Okamoto, T., Tokuya, T., & Takahashi, A. (1982). Solution properties and chain flexibility of pullulan in aqueous solution. *Biopolymers*, *21*, 1623–1633.
Kemp, M. M., & Linhardt, R. J. (2010). Heparin-based nanoparticles. *Nanomedicine and Nanobiotechnology*, *2*, 77–87.
Lara, H. H., Garza-Treviño, E. N., Ixtepan-Turrent, L., & Singh, D. K. (2011). Silver nanoparticles are broad-spectrum bactericidal and virucidal compounds. *Journal of Nanobiotechnology*, *9*, 30–37.
Lee, P. C., & Meisel, D. (1982). Adsorption and surface-enhanced raman of dyes on silver and gold sols. *Journal of Physical Chemistry*, *86*, 3391–3395.
Leung, T. C. Y., Wong, C. K., & Xie, Y. (2010). Green synthesis of silver nanoparticles using biopolymers, carboxymethylated-curdlan and fucoidan. *Materials Chemistry and Physics*, *121*, 402–405.
Li, S., Zhang, Y., Xu, X., & Zhang, L. (2011). Triple helical polysaccharide-induced good dispersion of silver nanoparticles in water. *Biomacromolecules*, *12*, 2864–2871.
Liu, J., He, F., Durham, E., Zhao, D., & Roberts, C. B. (2008). Polysugar-stabilized Pd nanoparticles exhibiting high catalytic activities for hydrodechlorination of environmentally deleterious trichloroethylene. *Langmuir*, *24*(1), 328–336.
Magudapatty, G., Gangopaghyayrans, P., Panigrahi, B. K., Nair, K. G. M., & Dhara, S. (2001). Electrical transport studies of Ag nanoparticles embedded in glass matrix. *Physica B: Condensed Matter*, *299*, 142–146.
Matthew, B., Dickerson, H., Sandhage, K., & Naik, R. R. (2008). Protein- and peptide-directed syntheses of inorganic materials. *Chemical Reviews*, *108*, 4935–4978.
Mendichi, R., Giammonab, G., Cavallarob, G., & Giacometti Schieronia, A. (2000). Molecular characterization of α,β-poly[(N-hydroxyethyl)-DL–aspartamide] by light scattering and viscometry studies. *Polymer*, *41*, 8649–8657.
Miranda, O. R., Creran, B., & Rotello, V. M. (2010). Array-based sensing with nanoparticles: Chemical noses' for sensing biomolecules and cell surfaces. *Current Opinion in Chemical Biology*, *14*, 728–736.
Picton, L., Bataille, G., & Muller, G. (2000). Analysis of a complex polysaccharide (gum arabic) by multi-angle laser light scattering coupled on-line to size exclusion chromatography and flow field flow fractionation. *Carbohydrate Polymers*, *42*, 23–31.
Portney, N. G., & Ozkan, M. (2006). Nano-oncology: Drug delivery, imaging, and sensing. *Analytical and Bioanalytical Chemistry*, *384*, 620–630.
Raveendran, P., Fu, J., & Wallen, S. L. (2003). Completely green synthesis and stabilization of metal nanoparticles. *Journal of the American Chemical Society*, *125*, 13940–13941.
Ravindran, A., Chandran, P., & Khan, S. S. (2012). Biofunctionalized silver nanoparticles: Advances and prospects. *Colloids and Surfaces B: Biointerfaces*, http://dx.doi.org/10.1016/j.colsurfb. 2012.07.036
Saito, T., & Isogai, A. (2004). TEMPO-mediated oxidation of native cellulose. The effect of oxidation conditions on chemical and crystal structures of the water-insoluble fractions. *Biomacromolecules*, *5*, 1983–1989.
Salkar, R. A., Jeevanandam, P., Aruna, S. T., Koltypin, Y., & Gedanken, A. (1999). The sonochemical preparation of amorphous silver nanoparticles. *Journal of Materials Chemistry*, *9*, 1333–1335.
Shibata, I., Yanagisawa, M., Saito, T., & Isogai, A. (2006). SEC-MALS analysis of cellouronic acid prepared from regenerated cellulose by TEMPO-mediated oxidation. *Cellulose*, *13*, 73–80.
Simakin, A. V., Voronov, V. V., Kirichenko, N. A., & Shafeev, G. A. (2004). Nanoparticles produced by laser ablation of solids in liquid environment. *Applied Physics A*, *79*, 1127.
Tamura, N., Hitora, M., Saito, T., & Isogai, A. (2010). Oxidation of curdlan and other polysaccharides by 4-acetamide-TEMPO/NaClO/$NaClO_2$ under acid conditions. *Carbohydrate Polymers*, *81*, 592–598.
Tamura, N., Wada, M., & Isogai, A. (2009). TEMPO-mediated oxidation of (1 → 3)-β-D-glucans. *Carbohydrate Polymers*, *77*, 300–305.
Venkatpurwar, V., & Pokharkar, V. (2011). Green synthesis of silver nanoparticles using marine polysaccharide: Study of in-vitro antibacterial activity. *Materials Letters*, *65*, 999–1002.
Watanabe, E., Tamura, N., Saito, T., Habu, N., & Isogai, A. (2012). Preparation of completely C6-carboxylated curdlan by catalytic oxidation with 4-acetamido-TEMPO. *Carbohydrate Polymers*, http://dx.doi.org/10.1016/j.carbpol. 2012.11.094
Wei, D., & Qian, W. (2008). Facile synthesis of Ag and Au nanoparticles utilizing chitosan as a mediator agent. *Colloids and Surfaces B: Biointerfaces*, *62*, 136–142.
Wu, J., Zhang, F., & Zhang, H. (2012). Facile synthesis of carboxymethyl curdlan-capped silver nanoparticles and their application in SERS. *Carbohydrate Polymers*, *90*, 261–269.
Xia, X., Monterio-Riviere, N., & Riviere, J. (2010). An index for characterization of nanomaterials in biological systems. *Nature Nanotechnology*, *5*, 671–675.
Xue, C., Meĭtraux, G. S., Millstone, J. E., & Mirkin, C. A. (2008). Mechanistic study of photomediated triangular silver nanoprism growth. *Journal of the American Chemical Society*, *130*(26), 8337–8344.
Yang, Y., Matsubara, S., & Xiong, L. (2007). Solvothermal synthesis of multiple shapes of silver nanoparticles and their SERS properties. *Journal of Physical Chemistry*, *111*, 9095–9104.